Earth Moon Planets (2012) 109:43–53
DOI 10.1007/s11038-012-9401-3

Varre-Sai: The Recent Brazilian Fall

M. E. Zucolotto · L. L. Antonello · M. E. Varela · R. B. Scorzelli · P. Munayco · E. dos Santos · Isabel P. Ludka

Received: 14 August 2012 / Accepted: 11 September 2012 / Published online: 22 September 2012

Abstract Varre-Sai, the most recent Brazilian meteorite fall, on June 19th, 2010 at Varre-Sai, in Rio de Janeiro State, Brazil (20°51′41″S; 41°44′.80″W). At least eight masses (total ~3.5 kg) were recovered. Most are totally covered by fusion crust. The exposed interior is of light-grey colour with a few dark shock veins. Five thin polished and etched sections were prepared from a slice weighing 35 g on deposit at the National Museum/UFRJ. It consists mostly of chondrules ranging in size from 0.35 to ~2.2 mm, and chondrule fragments enclosed in a crystalline matrix. The matrix consists of tiny isolated subhedral and anhedral crystals and opaque minerals that are intergrown with broken chondrules. The chondritic texture is poorly defined with chondrule textures that vary from non-porphyritic to porphyritic ones. The essential minerals are olivine ($Fa_{25\pm0.2}$) and low-Ca pyroxene ($Fa_{21.66\pm0.2}Wo_{1.4}$). Accessory minerals are plagioclase, apatite, Fe–Ni metal phases, troilite, chromite and magnetite. Mössbauer spectroscopy analysis confirms that the mineral phases are olivine, pyroxene, troilite and kamacite/taenite. Chemical data indicate that Varre-Sai is a member of the low iron L chondrite group. The observed texture and mineral phases led us to classify Varre-Sai as an equilibrated petrologic type 5. The shock features of the minerals (undulatory extinction, planar structure and numerous cracks), as well as plagioclase partial or totally transformed to maskelynite, suggest a shock stage S4. Also, some post-impact metamorphic processes could be inferred from the meta-sulfide conjoint grains that show complex mixtures of kamacite–taenite–tetrataenite and troilite. The occurrence of veins crosscutting the studied sections indicates that Varre-Sai was

M. E. Zucolotto
Museu Nacional/UFRJ, Rio de Janeiro, RJ, Brazil

L. L. Antonello · R. B. Scorzelli · P. Munayco · E. dos Santos
Centro Brasileiro de Pesquisas Físicas (CBPF/MCT), Rio de Janeiro, Brazil

M. E. Varela (✉)
ICATE-CONICET, Av España 1512 Sur, San Juan J5402DSP, Argentina
e-mail: evarela@icate-conicet.gob.ar

I. P. Ludka
Instituto de Geociências/UFRJ, Rio de Janeiro, RJ, Brazil

affected by a late fracturing event. Sealing of these fractures must have been a fast process, as shown by troilite globule textures pointing towards rapid solidification. The meteorite name was approved by the Nomenclature Committee of the Meteoritical Society (Meteoritic Bulletin, no 99).

Keywords Brazilian meteorite · Chondrite · Chondrules · Varre-Sai

1 Introduction

During the last 19 years there were no reports of meteorite falls in Brazil. The last was in 1991, when the fall of Campos Salles (an L6 ordinary chondrite) was recorded. In 2010, another meteorite fall was observed in the vicinity of Varre-Sai, Espírito Santo State. Five masses (with a total weight of $\sim$2.5 kg) were recovered and a single piece weighing 35 g was donated to the National Museum/UFRJ and is housed at the Department of Geology and Paleontology. Here, we present a detailed optical, chemical and Mössbauer spectroscopy study of the Varre-Sai chondrite. The meteorite name was approved by the Nomenclature Committee (NomCom) of the Meteoritical Society, Meteoritic Bulletin no 99 (2011).

2 Fall and Circumstances of the Recovery

On June 19th 2010, during the midday, a bright fireball was observed in a wide area, from Rio de Janeiro to Espírito Santo states (Brazil). Close to the fall locality, several explosions were heard by citizens which thought they were fireworks. Mr. Germano Oliveira was leaving his home when he looked up to the sky and noticed a rotating cloud and heard a big explosion that was rapidly followed by two others, further west. He continued walking and some minutes later he heard the whistling sound of a stone falling very close to him (almost hit him). Fifteen meters further, he heard a second stone. He was sure that something had fallen from the sky. The next morning, he began a search and found one of the stones that left a small mark on the ground. He showed the stone to his neighbors and transmitted the full story of the recovery. A boy who was a little suspicious asked the teacher, Rudolph Philomena, if it is possible that a stone could fall from the sky. Due to the intensive work performed in schools by one of us (M. E. Z: "Is there an ET in your backyard?"), spreading knowledge about meteorites and how to search for them, the National Museum of Rio de Janiero was contacted.

Antonio Campos, an amateur astronomer from CEAMIG (Centro de Estudios Astronómicos de Minas Gerais), also saw the fire-ball when he was on the road, some kilometers away from the place of the fall. He immediately launched a meteorite alert on the Internet and, fortunately, the fall was filmed from Alegre (a locality near Espirito Santo). According to the data collected by several witnesses and based on the film and one photograph, we can estimate that the bolide had an east–west trajectory.

Santa Rita do Prata (20°51′41″S; 41°44′80″W) is the exact location of the fall. This is a small village on the border of two states, distant 17 km from Varre-Sai (Rio de Janiero) and 8 km from Guaçuí (Epirito Santo). Because several stones were found on both sides of the border between the states, the proposed names were Varre-Sai or Varre-Sai-Guaçuí. The first was kept as the official name by the NomCom of the Meteoritical Society.

3 Materials and Methods

Five thin polished and etched sections were studied using optical microscope, scanning-electron microscopy (SEM), electron microprobe and Mössbauer spectroscopy. Optical microscopy was performed using a petrographic microscope Carl Zeiss, with Axionvision Release 4.7 software. SEM was performed on a Digital Scanning Microscope (DSM 940A Zeiss) equipped with a system for energy-dispersive X-ray micro-analysis (LINK/Oxford-exLII). Major element chemical compositions were obtained by an ARL-SEMQ (WDS) and a JXA-Jeol-8900 RL (WD/ED) electron microprobes with analyses acquired at conditions of 15 kV acceleration potential and 15 nA sample currents. Estimated precision for major and minor elements is better than 3 % and for Na about 10 %. Natural and synthetic standards were used for calibration and an online ZAF correction was applied to the data. The ^{57}Fe Mössbauer spectroscopy (^{57}Fe-MS) experiments were performed at room temperature in standard transmission geometry, using a 25 mCi ^{57}Co/Rh radioactive source in sinusoidal mode. The NORMOS code was used for spectrum analysis.

4 Petrography

In hand specimen almost all pieces are fusion crusted with regmaglypts of 1 cm in diameter and 2–4 mm deep. Broken surfaces expose a light grayish interior with few dispersed opaque minerals (some of which show magnetic susceptibility), scarce delineated oval and spherical chondrules and some dark shock veins (Fig. 1).

Under optical inspection Varre -Sai shows a chondritic texture similar to other ordinary chondrites with poorly defined chondrules often intergrown with the matrix (Fig. 2a). Chondrules, as well as the chondrule fragments, range in size from 0.35 to $\sim$2.2 mm in diameter. The matrix, formed mainly of mineral fragments, shows scarce areas with devitrified glass patches containing opaque minerals. The latter range in size from very fine-grained (re-crystallized matrix) to $\sim$0.9 mm in diameter. Several of the studied thin sections are transected by thin veins (Fig. 1) which appears dark in transmitted light. The thin veins are easily overlooked in reflective light as they appear as discontinuous thin (<200 μm) lines of troilite and kamacite.

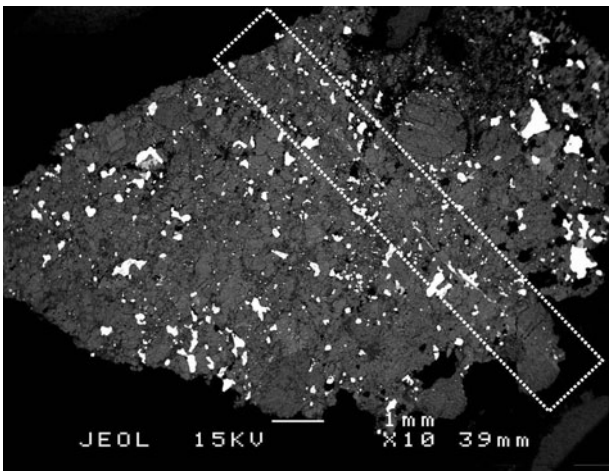

Fig. 1 Backscatter electron (BSE) image of a whole thin section showing the texture and distribution of the opaque phases in Varre-Sai. The thin section is crosscut by a thin vein (framed by the rectangular area in dotted white line). The thin veins are easily overlooked in reflected light as they appear as discontinuous thin (<200 μm) lines of troilite and kamacite

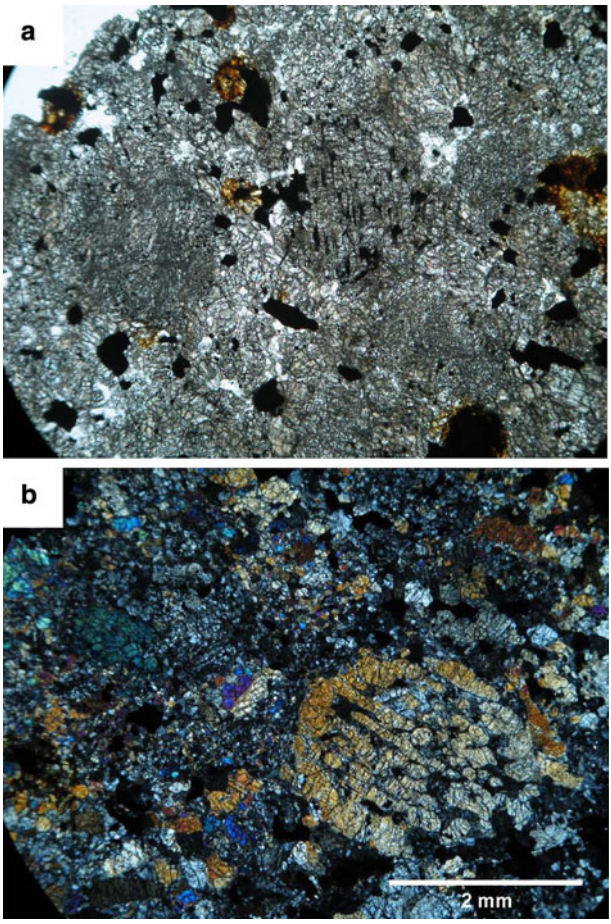

Fig. 2 Photomicrographs of Varre-Sai. **a** In transmitted plane polarized light showing the chondritic texture with poorly defined chondrules. Length of the field: 2.6 mm. **b** In cross polars light showing the near spherical shape of a barred olivine chondrule. *Scale bar*: 2 mm

Chondrules are more or less outlined and reveal a variety of internal textures varying from non-porphyritic to porphyritic ones (Gooding and Keil 1981) (Fig. 2). Although chondrules are often referred to as spherical or spheroid (Hughes 1978), many varieties of non-spherical porphyritic chondrules deviate from sphericity. These include chondrule fragments (Berkley et al. 1980) and porphyritic chondrules that contain phenocrysts that protrude slightly from the chondrule surface (King and King 1978).

The best preserved internal textures are observed in the non-porphyritic Radial Pyroxene (RP) (0.80–1.3 mm in length) and in Barred Olivine (BO) (0.30–2.1 mm in diameter) chondrules (Fig. 2b). Porphyritic olivine-pyroxene chondrules (POP) range from 0.8 mm to about 2.1 mm in apparent diameter. In a large object, a fractured subhedral skeletal olivine crystal with interstitial small grains of olivine, plagioclase and pyroxene grains was observed. Granular olivine-pyroxene chondrules (GOP) consist of closely packed olivine and pyroxene grains. Some of the olivine grains are packed among each other with strong mosaicism with multiple sets of parallel planar fractures and planar deformation.

There are several POP chondrules fragments within the matrix composed of large olivine or pyroxene crystals showing undulatory extinction, planar structure and numerous cracks. The chondrule fragments are often surrounded by opaque minerals.

The matrix is composed of olivine, pyroxene and plagioclase. The latter is partial or completely transformed into maskelynite. The distribution of opaque minerals is concentrated mainly along chondrule boundaries and within the matrix.

5 Mineral Chemistry

5.1 Major Element Phase Compositions

The essential minerals are olivine and low-Ca pyroxene with minor amounts of plagioclase, twinned clinopyroxene, apatite, troilite, Fe–Ni metal, chromite, troilite, magnetite, and turbid devitrified glass. Representative analyses of major and accessory mineral phases are given in Tables 1, 2 and 3.

Olivine (Fa_{25}) typically has FeO contents between 22.4 and 22.9 wt%. The MnO contents vary between 0.40 and 0.50 wt%. Pyroxenes are low-Ca pyroxene ($Fs_{21.66}Wo_{1.4}$) with FeO contents varying from 13.7 to 14.2 wt%, TiO_2 and CaO in the range of 0.15–0.32 wt% and 0.52–0.79 wt%, respectively, with Cr_2O_3 from 0.08 to 0.19 wt%.

5.2 Accessory Minerals

Plagioclase occasionally shows polysynthetic twins and most grains display plastic deformation as evidenced by undulatory extinction and partial isotropization (some are completely transformed into diaplectic glass maskelynite). For shock classification we have only considered the complete transformation of plagioclase grains to maskelynite (e.g., Rubin 1997). Plagioclases are albitic in composition ($Ab_{82.4}$ to $Ab_{79.1}$) with Na_2O contents that vary from 9.05 to 7.38 wt%, respectively. Very scarce apatite grains were observed. The major element compositions of accessory phases are given in Table 3.

The main Fe–Ni metal grains (kamacite and taenite) are typically irregular in shape (Fig. 3a, b). The presence of Neumann lines and Widmanstätten-like patterns was only observed in large fragments of kamacite which, in addition, show a polycrystalline texture. In some grains the border between kamacite and taenite is decorated by tetrataenite. A compositional profile performed across this border (Fig. 3a) show the wide variation in Ni content in kamacite ($\sim$5 wt% Ni), tetrataenite (49–52 wt% Ni) and taenite (16–35.9 wt% Ni) (Table 4). In etched samples, some metallic grains show a dark cloudy plessite core rimmed by tetrataenite.

Table 1 Representative electron microprobe analyses (EMPA) of olivine (wt%)

SiO_2	38.6	38.6	38.2	38.7	38.4	38.3	38.0	38.2
Cr_2O_3	0.00	0.03	0.05	0.00	0.00	0.00	0.03	0.05
FeO	22.7	22.8	22.7	22.2	22.9	22.8	22.4	22.8
MnO	0.40	0.44	0.44	0.50	0.47	0.44	0.45	0.50
MgO	38.1	37.9	38.1	38.7	38.2	37.9	37.8	37.6
Total	99.8	99.8	99.5	100.0	99.9	99.5	98.7	99.1

Table 2 Representative electron microprobe analyses (EMPA) of pyroxene (wt%)

SiO_2	55.3	55.3	55.6	55.4	55.5	55.5	55.5	55.6	55.5	55.5
TiO_2	0.32	0.24	0.24	0.20	0.18	0.15	0.20	0.20	0.18	0.18
AI_2O_3	0.25	0.21	0.17	0.18	0.18	0.15	0.14	0.14	0.19	0.15
C_2O_3	0.19	0.15	0.08	0.11	0.09	0.09	0.10	0.09	0.13	0.11
FeO	13.7	13.8	14.1	14.0	14.0	14.0	13.9	14.0	14.1	14.2
MnO	0.46	0.48	0.45	0.50	0.51	0.45	0.45	0.47	0.48	0.46
MgO	28.3	28.6	28.7	28.7	28.4	28.7	28.6	28.8	28.7	28.5
CaO	0.79	0.76	0.76	0.75	0.73	0.65	0.72	0.52	0.70	0.70
Total	99.4	99.6	100.1	99.9	99.7	99.7	99.6	99.8	100.0	99.9

Table 3 Representative EMPA of accesory phases (wt%)

	Plag.	Plag.	Plag.	Apatite
SiO_2	65.7	65.7	65.9	0.77
TiO_2	0.04	0.08	0.05	0.11
Al_2O_3	22.2	22.1	22.6	
Cr_2O_3	0.00	0.00		
FeO	0.40	0.30	0.67	1.03
MnO	0.03	0.00	0.01	0.34
MgO	0.00	0.00	0.01	0.13
CaO	2.22	2.16	2.29	56.4
Na_2O	9.05	8.72	7.38	0.40
K_2O	1.07	1.48	1.04	
P_2O_5				40.7
Total	100.7	100.6	99.9	99.9
Ab	82.4	80.1	79.1	
An	11.2	11.0	13.6	
Or	6.4	8.9	7.3	

Troilite grains have angular to sub-rounded shapes ranging in size from a few microns up to 0.1–0.8 mm. They occur disseminated in the matrix or can also rim almost an entire chondrule. Metal and sulfide can form conjoined grains. In this case, the metal-sulfide contact can be clean with smooth surfaces (Fig. 3b) or highly irregular with sulfides protruding inside the metal. The latter also exhibit a complex intergrowth mixture of troilite, tetrataenite and Fe–Ni metal (Fig. 3c). Coarse-plessite textures, partially surrounded by tetrataenite, are distinguished within the metallic portion where many small troilite inclusions are present. The contacts between troilite and metal are tetrataenite-rich (Fig. 3c; Table 5).

Chromite occurs in small grains associated with troilite and silicate phases, mainly olivine. Magnetite occurs in rounded and angular small grains within silicates.

Mössbauer analysis of the Varre-Sai bulk sample showed a spectrum composed of overlapping paramagnetic and magnetic phases. The spectra at room temperature exhibits two Fe^{2+} doublets attributed to olivine and pyroxene, and additionally two magnetic phases associated with Fe–Ni phases (kamacite and/or taenite) and troilite (Fig. 4).

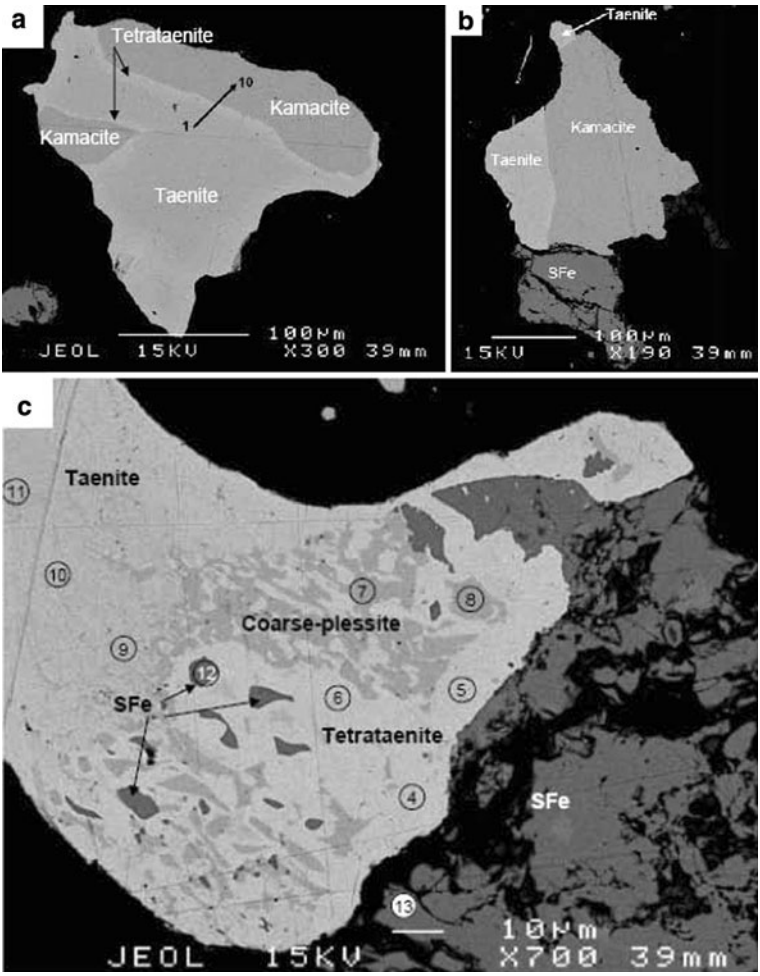

Fig. 3 BSE images of: **a** a metal grain showing the distribution of taenite and kamacite rimmed by tetrataenite. *Dark arrow* (1–10) indicates location of the profile (Table 4). **b** Metal (kamacite and taenite) and sulfide (SFe) conjoint grain. Note the clean metal-sulfide contact forming a smooth surface. **c** Metal-sulfide contact showing a complex intergrown mixture of troilite, tetrataenite and Fe–Ni metal. The latter can develop a coarse-plessite texture where several small troilite inclusions are present. The encircled numbers correspond to the microprobe analysis, as indicated in Table 5

Table 4 Representative electron microprobe analyses of metal (wt%)

	1	2	3	4	5	6	7	8	9	10
Fe	83.3	82.8	82.3	73.9	63.6	49.5	47.6	93.3	93.7	93.5
Co	0.71	0.63	0.71	0.44	0.29	0.18	0.15	0.77	0.90	0.79
Ni	16.2	16.5	16.0	26.1	35.9	49.0	52.2	5.1	5.0	4.9
Total	100.2	99.9	99.0	100.4	99.8	98.7	100.0	99.1	99.6	99.2

Table 5 Representative electron microprobe analyses of metal and sulfide (wt%)

	4	5	6	7	8	9	10	11	12	13
S									36.0	36.0
Fe	47.1	47.7	46.9	95.2	94.0	77.7	78.2	66.2	64.1	63.8
Co	0.10	0.11	0.11	1.40	1.28	0.90	0.86	0.41		
Ni	53.1	51.7	53.5	4.1	5.5	22.0	21.8	32.9	0.71	
Total	100.3	99.5	100.5	100.7	100.8	100.6	100.9	99.5	100.8	99.8

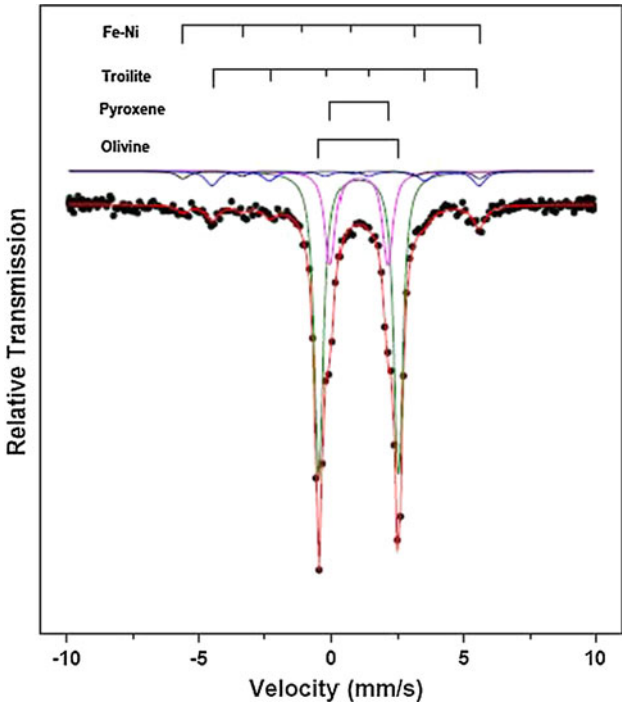

Fig. 4 The ^{57}Fe Mössbauer spectra performed at room temperature, the bulk sample shows kamacite, troilite, olivine and pyroxene

6 Discussion and Conclusions

Varre-Sai consists of chemically homogeneous (in terms of Fe and Mg) major phases (Tables 1, 2). Taking into account the average composition of olivine ($Fa_{25\pm0.2}$) and low-Ca pyroxene ($Fa_{21.66}$), it can be classified as a member of the L chondrite group (e.g., Brearley and Jones 1998). The texture shows poorly delineated chondrules with presence of clinopyroxene, apatite, plagioclase and devitrified turbid glass indicating a petrologic type 5 (Fig. 5) (Van Schmus and Wood 1967; Rubin 1990).

Varre-Sai has ambiguous features indicating variable shock stages in the same Chondrite. On the one hand it shows deformation features (such as planar fractures and undulatory extinction in plagioclase and olivine, partial or complete transformation of

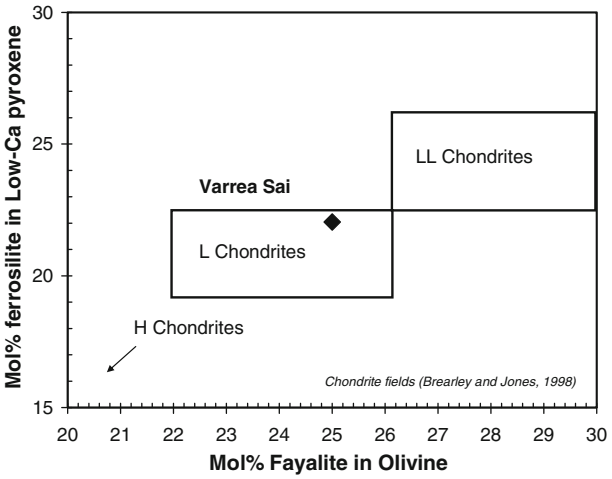

Fig. 5 Classification of Varre-Sai considering the average of Low-Ca pyroxene and olivine. Chondrites fields from Brearley and Jones (1998)

plagioclase to maskelynite and fractures affecting most silicate grains) suggesting a shock stage S4 (Stoffler et al. 1991). On the other hand, the highly homogeneous chemical composition of plagioclase is a feature that is mainly observed in unshocked ordinary chondrites. However, the slow diffusion rates of NaSi-CaAl substitutions (Hart 1981) could explain the presence of plagioclase with uniform compositions in highly shocked chondrites.

According to McSween et al. (1988), type 4–6 ordinary chondrites experience metamorphic heating up to peak temperatures between 700 and 900 °C. Based on Fe–Mg exchange between olivine and spinel, Kessel et al. (2007) found that the average equilibration temperatures (the lowest temperature for solid state diffusion) for a suite of H, L, LL ordinary chondrites with petrologic types 4–6, cover a narrow range between 586 and 777 °C, as compared with previous determination of metamorphic temperatures (e.g., <600–950 °C, Heyse 1978). Clearly the mineral thermometers can give closure temperatures below the peak metamorphic conditions (e.g., for type 6 ordinary chondrites, Kessel et al. 2007). To overcome this problem, the study of metal-sulfide textures (Scott 1982; Tomkins 2009) seems to have the potential to record minimum temperature variations. Similar textures to those observed in metal-sulfide assemblages in Varre-Sai (Fig. 3c), but in which Cu was also observed, are explained as the result of two processes: (1) shock melting, followed by annealing, of the metal-sulfide assemblage (Rubin 2004), or (2) the result of low temperature exsolution from a high temperature sulfide solid solution phase contained within the metal (an unrelated shock feature, e.g., El Goresy 2006). An alternative process has been recently proposed by Tomkins (2009) in which these textures could be formed as the product of sub-solidus chemical transfer (e.g., sulphur migration into metal) during post-impact metamorphism. Accordingly, the small inclusions of troilite, typically rimmed by taenite or tetrataenite, could form by diffusion of sulphur from the adjacent troilite along structural defects at high temperatures (Tomkins 2009). Under such a process the metal component of the composite metal-troilite grains will contain <25 % of troilite inclusions in the plessite texture (as observed in Varre-Sai conjoint grains, Fig. 3c). The low abundance of troilite (<25 %) suggests that the mixed metal-troilite domain is far from the Fe-FeS eutectic or Fe–Ni–FeS cotectic compositions and thus does not represent an annealed melt (e.g., Tomkins 2009). Consequently, these textures could be the result of high temperature events possibly approaching 850 °C. The presence in the same thin

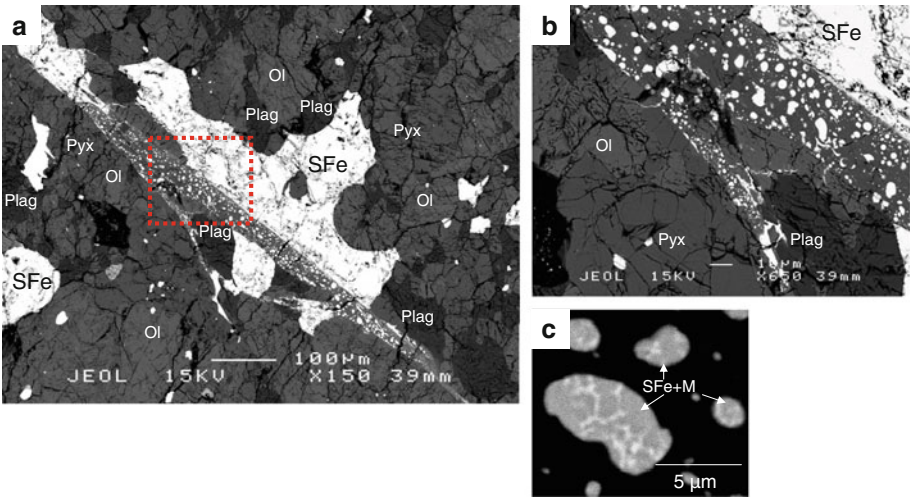

Fig. 6 BSE images, **a–b** showing details of the thin veins that crosscut the thin section. Note the abundance of troilite globules. **c** Detail of a troilite globule showing the dendrite-like or cellular-like texture formed by Ni-rich metal (bright clear *grey*)

section of conjoint grains showing net borders (Fig. 3b) puts some constraints on the magnitude of the heating and clearly indicates that this process was heterogeneous, giving support to the fact that the presence of ambiguous features indicating variable shock stages (in the same chondrite) is common.

The occurrence of veins that crosscut the studied sections is another feature pointing towards a later deformation event (Figs. 1, 6a, b). The chemical composition of the minerals inside the vein resembles that of the main constituents of the chondrite (e.g., olivine and pyroxene in the vein have low SiO_2 contents with slightly lower contents of FeO and MgO). However, in plagioclase sodium contents are reduced by half and at least one pyroxene shows high contents of Al_2O_3, CaO and Na_2O (Table 6). The troilite globules inside the veins are very small and show dendrite-like or cellular-like textures (bright clear grey, Fig. 6c) formed by Ni-rich metal. This texture resembles that observed

Table 6 Representative EMPA of mineral phases in the vein (wt%)

	Olivine	Olivine	Pyroxene	Pyroxene	Plagioclase	Plagioclase
SiO_2	36.9	36.0	48.1	53.4	65.6	65.9
TiO_2	0.00	0.00	0.09	0.17	0.06	0.11
Al_2O_3	0.02	0.00	4.71	0.17	21.6	21.2
Cr_2O_3	0.00	0.06	0.16	0.06	0.00	0.31
FeO	21.2	22.3	14.6	13.3	0.81	0.85
MnO	0.43	0.32	0.30	0.43	0.00	0.06
MgO	35.8	34.9	23.9	27.3	0.02	0.00
CaO	0.04	0.00	2.01	0.68	1.92	1.84
Na_2O	0.03	0.50	1.34	0.00	3.05	4.90
K_2O	0.08	0.05	0.14	0.08	0.70	0.97
Total	94.5	94.1	95.3	95.5	93.7	96.1

in rapidly solidified metallic spherules enclosed in troilite from the San Emigdio H4 chondrite (Scott 1982), suggesting that sealing of these fractures was a rapid event that possibly took place on the surface of the carrier body.

The recent Brazilian fall Varre-Sai is thus classified as an equilibrated ordinary chondrite (L5) with shock stage S4 and a degree of weathering W0. The meteorite name was approved by the NomCom of the Meteoritical Society (Meteoritic Bulletin, no 99).

Acknowledgments The manuscript benefited from the comments of H. Downes. Financial support was received from FAPERJ (E. Zucolotto), Agencia (PICT 0142) and CNPQ during scientific visits to CBPF (M. E. Varela). R. B. Scorzelli would like to thank FAPERJ and CNPq for financial support; P. Munayco and E. dos Santos are grateful to FAPERJ and CAPES and L. L. Antonello to CBPF/MCT for their fellowships.

References

J.L. Berkley, G.J. Taylor, K. Keil, Geochim. Cosmochim. Acta **44**, 1579–1597 (1980)
A.J. Brearley, R.H. Jones, Chondritic meteorites, in *Planetary Materials*, ed. by J.J. Papike (Mineralogical Society of America, Washington, 1998), pp. 3.1–3.398
A. El Goresy, Meteorit. Planet Sci. **41**, A204 (2006)
J.L. Gooding, K. Keil, Meteoritics **16**, 17–43 (1981)
S.R. Hart, Geochim. Cosmochim. Acta **45**, 279–291 (1981)
D.W. Hughes, Earth Planet. Sci. Lett. **38**, 391–400 (1978)
J.V. Heyse, Earth Planet. Sci. Lett. **40**, 365–381 (1978)
R. Kessel, J.R. Beckett, E.M. Stolper, Geochim. Cosmochim. Acta **71**, 1855–1881 (2007)
T.V.V. King, E.A. King, Meteoritics **13**, 47–72 (1978)
H.Y. McSween, D.W.G. Sears, R.T. Dodd, Thermal metamorphism, in *Meteorites and the early solar system*, ed. by J.F. Kerridge, M.S. Mathews (University of Arizona Press, Tucson, 1988), pp. 102–113
E. Rubin, Geochim. Cosmochim. Acta **54**, 1217–1232 (1990)
A.E. Rubin, Meteorit. Planet. Sci. **32**, 231–247 (1997)
A.E. Rubin, Geochim. Cosmochim. Acta **68**, 673–689 (2004)
E.R.D. Scott, Geochim. Cosmochim. Acta **46**, 813–823 (1982)
D. Stoffler, K. Keil, E.R.D. Scott, Geochim. Cosmochim. Acta **55**, 3845–3867 (1991)
A.G. Tomkins, Meteorit. Planet. Sci. **44**, 1133–1149 (2009)
W.R. Van Schmus, J.A. Wood, Geochim. et. Cosmochim. Acta **31**, 747–765 (1967)